

GEMINATE AND NON-GEMINATE RECOMBINATION IN a-Si:H: OLD QUESTIONS AND NEW EXPERIMENTS

W. Fuhs*

Hahn-Meitner-Institut Berlin, Kekuléstraße 5, D-12489 Berlin, Germany

Radiative recombination in a-Si:H at 1.4 eV is associated with recombination between electrons and holes trapped in the respective bandtails. According to the widely accepted radiative tunneling model two recombination regimes are to be expected with different kinetics: Geminate recombination at low and moderate generation rates and non-geminate distant pair recombination at high generation rates. However, both at high- and low generation rates the observations appear to be in conflict with the radiative tunneling model. The present models are discussed in view of results from frequency resolved spectroscopy (FRS) and recent investigations of pulsed optically detected magnetic resonance (PODMR). These studies show that geminate and non-geminate recombination coexist in a-Si:H. The radiative recombination channels have been identified by PODMR as exchange coupled pairs (excitons) and strongly dipolar coupled electron hole pairs.

(Received July 4, 2005; accepted July 21, 2005)

Keywords: Amorphous silicon, Recombination, Lifetime spectra, Radiative tunneling, Exciton, Distant pairs

1. Introduction

The research in the field of amorphous semiconductors from the early beginning has been driven by both the scientific interest in basic aspects of disorder in the properties of solids and technological applications. In the early years chalcogenide glasses were in the center of the interest due to thin-film applications in imaging, xerography, memory and switching devices. By then amorphous silicon and amorphous germanium, a-Si and a-Ge, were of more academic scientific interest. The early forms of amorphous silicon had unacceptable electronic properties due to a high density of states in the energy gap which effectively pinned the Fermi level. Such material properties prevented this material from being useful for electronic devices. This situation changed when at the beginning of the seventies plasma enhanced chemical vapor deposition (PECVD) came into use which enabled the preparation of hydrogenated films with attractive semiconducting properties. Six milestones may be seen in the material and device development which led to a burst of research activities in this field and to exciting technological applications:

- Introduction of plasma enhanced chemical vapor deposition (PECVD) by Chittick, Alexander and Sterling in 1969 [1].
- Discovery that the defect density in this new kind of amorphous silicon was low which resulted in high photoconductivity [2].
- Demonstration of hydrogen passivation in sputtered a-Si:H and a-Ge:H [3].
- Successful substitutional n-type and p-type doping by addition of phosphine or diborane to the process gas by LeComber and Spear [4].
- First report on photovoltaic solar cells from a-Si:H by Carlson and Wronski in 1976 [5].
- First report on the fabrication and physics of a thin-film transistor by LeComber, Spear, and Gaith [6].

* Corresponding author: fuhs@hmi.de

Today, hydrogenated amorphous silicon, a-Si:H, offers a mature material and device technology used for solar cells, thin-film transistors, sensors, imaging, radiation detectors and displays [7,8]. The research efforts in this field therefore have strongly shifted to device and process technology. In spite of this tremendous development important scientific questions are still open and under investigation. Examples are the thermodynamics of the phase transitions in a-Si, the relationship between the local structure and the exponential tail states, the Hall effect anomaly, the various forms of metastability, or the nature of excess carrier recombination at low temperatures. This paper will discuss the present understanding of radiative recombination in the light of recent results from frequency resolved spectroscopy (FRS) and pulsed optically detected magnetic resonance (PODMR).

2. Density of states distribution

Numerous experimental techniques have been applied for the investigation of intrinsic and extrinsic defect states which led to the model depicted in Fig. 1. A characteristic of amorphous semiconductors is the disorder-induced localization of states near the band edges. From the mobility edges E_C and E_V tails of localized states extend deep into the gap with an exponential energy distribution. Although the existence of exponential band tails is well established, it is experimentally unclear how far the exponential tails extend towards the mobility edges and how deep they reach into the energy gap. It is also an open question why the localized-state-distribution is exponential at all. Thus the relationship between structural disorder and the exponentially distributed band tail states is still unclear.

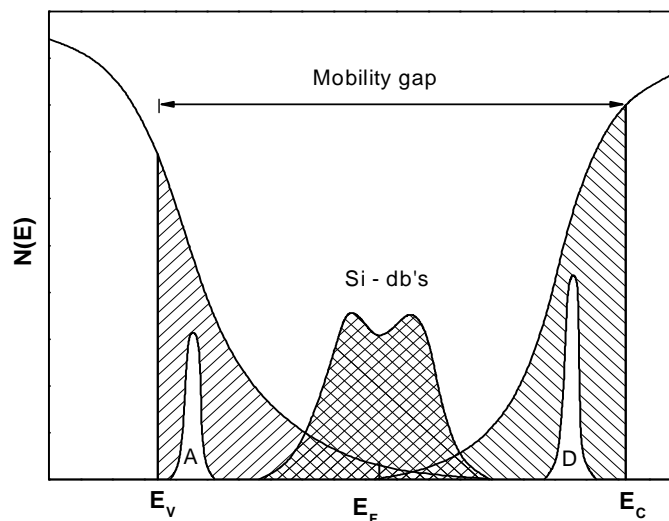


Fig. 1. Model density of states distribution in hydrogenated amorphous silicon a-Si:H. E_C and E_V denote the mobility edges in the conduction and valence band.

Deep defect states are formed as a result of stress release in the amorphous network but may also arise from unfavorable deposition conditions. The simplest point defect is an unsaturated Si bond for which the term Si-dangling bond is generally used. The positive/neutral state of this defect is located around midgap in undoped material, the negatively charged state is shifted to higher energy by a positive correlation energy U of about 0.2 eV. In electron spin resonance (ESR) three resonances have been observed which are associated with states in different regions of the energy gap. The signal in undoped or weakly doped a-Si:H at $g = 2.0055$ has been assigned to the neutral three-fold coordinated Si atom which has a free sp^3 hybrid orbital (Si-dangling bond, Si-db). When the band tails are populated by doping or illumination additional signals appear at $g = 2.0043$ and $g = 2.012$ due to localized band tail electrons and holes, respectively.

For many years it was believed that the density-of-states distribution is a stable property of a-Si:H. This, however, is not the case: $N(E)$ can vary with temperature, doping level, carrier injection, or light absorption. The density and energy distribution of the defects is determined by the position of the Fermi level E_F and therefore $N(E)$ changes whenever and by whatever E_F is moved in films and devices.

3. The radiative tunneling model and frequency resolved spectroscopy

The temperature dependence of the photoconductivity and the photoluminescence of a-Si:H (Fig. 2) suggest to distinguish two temperature ranges. At $T < 60$ K the photoluminescence intensity I_{PL} is very high with a quantum efficiency close to unity, the photoconductivity σ_{PH} is very small and both quantities do not depend on temperature. σ_{PH} depends linearly on the generation rate and varies only little with the defect density or doping level. This mechanism of photoconduction appears to be a universal feature for amorphous semiconductors and was assigned to hopping in the tail states [9]. A theory of hopping photoconduction has been developed for finite temperatures and high electric fields which led to a satisfactory explanation of these observations [10]. These theories suggest that as a result of excitation to higher band tail states a transport path develops in the band tail at an energy E_t which moves as a function of temperature and electric field strength to higher energy. At $T > 100$ K the transport channel has moved into the extended states and transport is considered to occur at the mobility edge. In this range the dependence on the generation rate, the magnitude of σ_{PH} and the detailed kinetics are determined by the occupancy of the defect states.

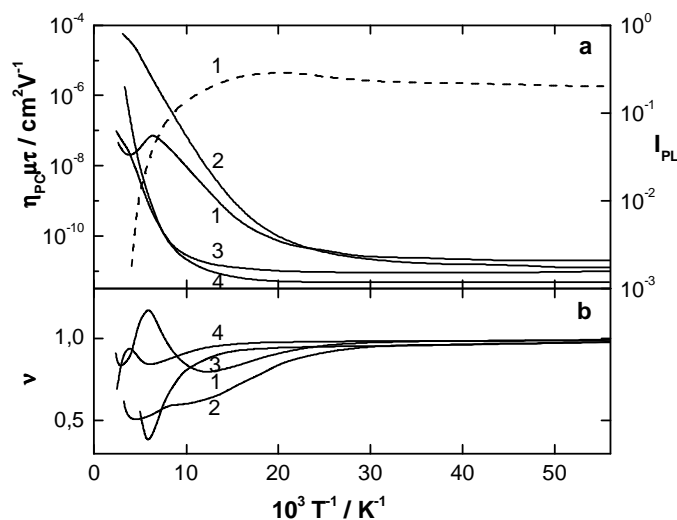


Fig. 2. Temperature dependence of the normalized photoconductivity $\eta_{PC}\mu\tau$ (a) and of the exponent ν of the intensity dependence $\sigma_{PH} \approx G^\nu$ of various a-Si:H films [9]. PECVD-films: (1) undoped, (2) 100 vppm PH_3 , (3) 1000 vppm B_2H_6 ; sputtered film: (4) undoped. The dashed line shows the temperature dependence of the photoluminescence intensity I_{PL} (sample 1).

The interpretation of such data requires information on the dominating recombination and transport paths, the density and energy distribution of the participating states. In addition one has to consider the random location of the states in space. The intensive work on photoluminescence, photoconductivity and in particular spin-dependent recombination as studied by optically detected magnetic resonance (ODMR) and electrically detected magnetic resonance (EDMR) have provided evidence that Si dangling bonds are the most effective centers for non-radiative recombination in the entire temperature range.

The photoluminescence spectrum of a-Si:H with low defect density exhibits a single structureless emission band centered at 1.3 – 1.4 eV with a half width of 0.25-0.3 eV which is

associated with recombination between electrons and holes in the band tail. The quantum efficiency of this intrinsic emission can be very high, the reported values amount to 0.3 – 1 for optimized films [11]. In defect rich or highly doped films this intrinsic band is quenched and an additional structure appears at 0.8 – 0.9 eV which is somewhat broader (0.35 – 0.4 eV) and has a much lower efficiency. The recombination kinetics are characterized by a broad distribution of lifetimes which extends from $10^{-8} - 10^{+2}$ s with an average lifetime of $\tau \approx 10^{-3}$ s at moderate generation rates [11, 12, 13, 14]. This experimental experience led to the proposal of models which have in common that the carriers recombine by radiative tunneling between tail states such that the broad distribution of lifetimes results from a distribution of pair separations. In the geminate pair model it is assumed that diffusion during thermalization does not separate the photoexcited electrons and holes such that recombination occurs between e-h pairs which have been created in the same absorption event. In the distant pair model it is supposed that the carriers are able to diffuse apart and recombine radiatively with the nearest available partner in a non-geminate process. When the generation rate G increases there should be a transition from geminate to non-geminate recombination connected with a change in the kinetics. At low G the lifetime distribution of geminate pairs is independent of the generation rate whereas at high G the lifetime distribution is expected to shift to shorter times with increasing G due to the strong decrease of the lifetime with increasing carrier concentration. This in fact is found in experiment (Fig. 3).

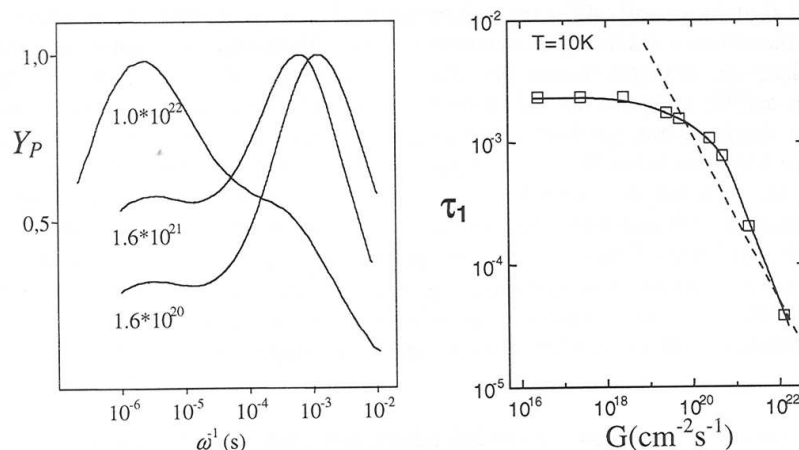


Fig. 3. (a) FRS lifetime spectra (normalized to peak height) of a-Si:H [13] (10 K, parameter G). (b) Position of the main peak τ_1 as a function of the generation rate G [12]. The dashed line is a theoretical curve for distant pair recombination [18].

The theoretical description of the radiative tunneling model starts from the assumption that photogenerated pairs diffuse apart by thermalization in the tail states which proceeds by hopping transitions. The rate for a hop over a distance r to a state of lower energy is given by

$$v = v_0 \exp(-2r/a) \quad (1)$$

with a prefactor $v_0 \approx 10^{12} \text{ s}^{-1}$ and the Bohr radius a of the band tail electron. When the electron hops to a state which is higher in energy by ΔE , this rate has to be multiplied by $\exp(-\Delta E/kT)$. Thermalization competes with radiative tunneling, the rate of which is described by

$$v = \tau_0^{-1} \exp(-2R/a) \quad (2)$$

In this expression R denotes the inter-pair separation and the prefactor is assumed to be $\tau_0 \approx 10^{-8} \text{ s}^{-1}$ as is typical for an allowed dipole transition. Due to the difference of the prefactors by four orders of magnitude the final radiative transition is the rate limiting step of the overall process and therefore the radiative lifetime is given by the inverse of the recombination rate

$$\tau_r = \tau_0 \exp (2R/ a) \tag{3}$$

This model relates the broad distribution of radiative lifetimes with the distribution of pair separations and is referred to as radiative tunneling model. The model appears to be supported by the characteristic dependence of the lifetime distribution on the generation rate G . The spectra measured by frequency resolved spectroscopy (FRS) show a major component at $\tau_1 \approx 1$ ms and a minor contribution at $\tau_2 \approx 1$ μ s both of which are independent of G at low excitation densities ($G < G_{crit} \approx 5 \times 10^{19}$ cm⁻³s⁻¹) suggesting the predominance of geminate recombination. The spectra shifts to shorter times at high values of G when the pair concentration is high such that the pairs overlap and recombination follows distant pair kinetics. Fig. 3a presents examples for spectra at high generation rates and Fig. 3b shows the dependence of the main peak at 1 ms on the generation rate.

The radiative tunneling model leads to predictions which are difficult to reconcile with the experimental results both at low and high generation rates. The first problem is that the model as discussed above is not consistent with the existence of geminate recombination. Computer simulations on basis of the above model [15, 16] considering the competition between thermalisation and radiative recombination showed that the e-h pairs diffuse appart to very large distances which in a cw experiment results in prevailing non-geminate recombination which follows distant pair kinetics. The calculated lifetime distribution shifts monotonously to shorter times with increasing G which is in contradiction with the observed behavior (see Fig. 3). At high generation rates a number of experiments show that the PL-intensity increases sublinearly with G at high excitation densities $G > G_{crit} \approx 5 \times 10^{19}$ s⁻¹cm⁻³ [11, 13]. A detailed study of frequency resolved spectroscopy led unambigiously to the conclusion that this behavior and the shortening of the lifetime at high values of G are , different from the expectation of the radiative tunneling model, entirely induced by the competition of a non-radiative channel [13].

This failure of the radiative tunneling model led to the suggestion that only the geminate process is radiative while distant pair recombination is non-radiative [17]. In this approach the lifetime spectrum was calculated assuming competition between these processes on basis of the model functions for the respective processes shown in Fig. 4. The lifetime spectrum of the geminate process was derived from the experiment at low generation rate and the spectra of distant pair recombination were taken from the analytical theory of Dunstan [18]. This assumption led to a quantitative description of the observed influence of the generation rate on the lifetime spectra (Fig. 5). The calculated dependence of the position of the two bands in the lifetime spectra ($\tau_1 \approx 1$ ms and $\tau_2 \approx 1$ μ s) on G and of the decrease of the partial quantum efficiencies as shown in Fig. 6 is in good accordance with the experiment. However, the question remained unanswered what the physical difference between geminate pairs and distant pairs might be.

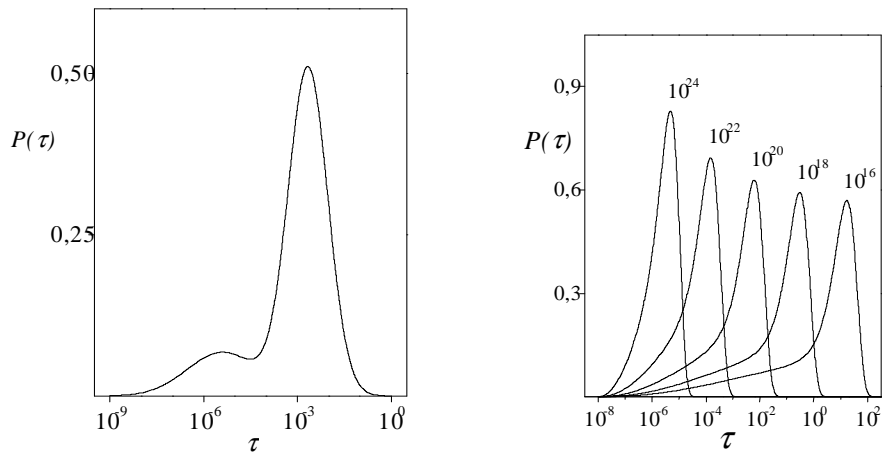


Fig. 4. Model functions for the lifetime spectra: (a) geminate recombination with peaks at $\tau_1 \approx 1$ ms and $\tau_2 \approx 1$ μ s [17], (b) non-geminate recombination [18]. Parameter G in (b) is the generation rate G .

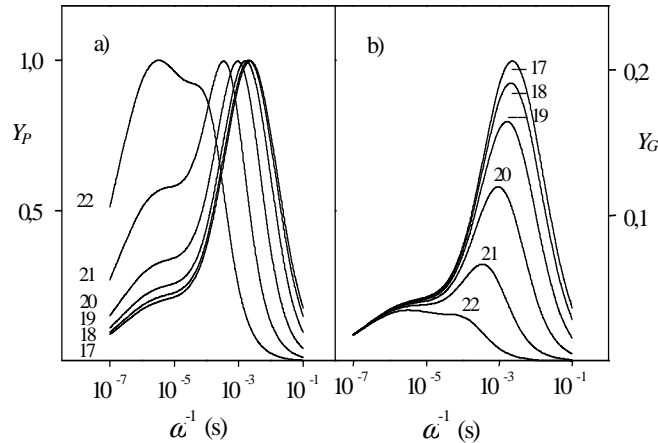


Fig. 5. Calculated lifetime spectra assuming that geminate recombination is radiative while non-geminate distant pair recombination is non-radiative [17]. (a) normalized to the peak maximum, (b) normalized to the generation rate to show the decrease of the PL-intensity at high G.

A recent FRS investigation suggests that different from the above assumption distant pair recombination is radiative [14]. The FRS spectra (Fig. 7) measured well in the range of geminate recombination ($G < 5 \times 10^{19} \text{ cm}^{-3} \text{ s}^{-1}$) reveal an additional band at long times of $10^{-2} - 10^2 \text{ s}$. Whereas the main component remained located at 1 ms, this band shifts with increasing G to shorter times as one expects for the distant pair process until it merges into the main peak at 1 ms. These results show that at low G geminate and non-geminate recombination coexist. In fact this is what has been discussed since long. Light induced electron spin resonance measures the steady state carrier concentration in the band tail. In the entire range of generation rates G the spin density n_s is found to increase sublinearly following a power law $n_s \propto G^\nu$ with $\nu \approx 0.17 - 0.2$. Such behavior is very characteristic for distant pair recombination [11, 18] and is due to the pronounced shortening of the lifetime when the pair separation decreases with increasing carrier concentration. This dependence has been shown to be valid also in the region of low G where radiative recombination follows geminate kinetics [12]. It was therefore concluded that photoluminescence and LESR measure carriers in different ranges of the lifetime spectrum.

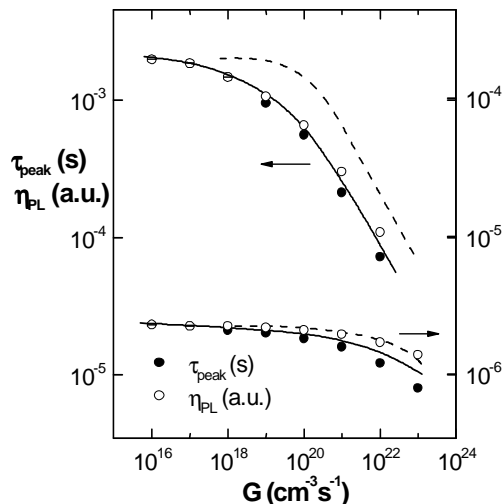


Fig. 6. Calculated positions and partial efficiencies (symbols) of the channels at τ_1 and τ_2 . The dashed curves: experimental result [13].

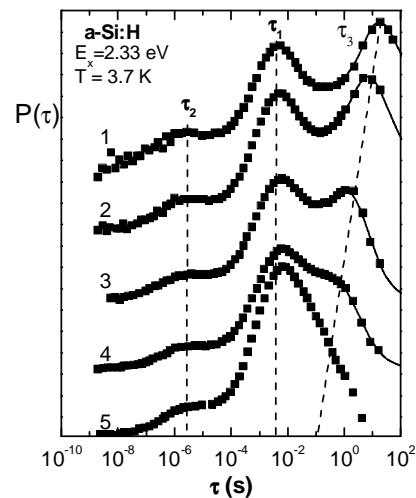


Fig. 7. FRS lifetime spectra measured at various generation rates [14]. $G(\text{cm}^{-3} \text{ s}^{-1})$: (1) 2.5×10^{15} , (2) 1.3×10^{16} , (3) 6.5×10^{16} , (4) 2.8×10^{17} , (5) 1.3×10^{18}

The lifetime spectra from FRS spectroscopy show regimes with predominant geminate and non-geminate kinetics. They support the view that geminate and non-geminate recombination are both radiative processes. FRS spectroscopy has shown that a non-radiative process becomes effective at high generation rates the nature of which is still an open question. Auger recombination appears to be a rather unlikely explanation in view of the low generation rates where this process becomes active. An additional argument against the dominance of Auger recombination comes from the observation that the LESR spin density increases sublinearly also at high G. This shows that distant pair kinetics determine the lifetime and the steady state carrier concentration. Although such investigations give insight into the kinetics of recombination they are unable to identify the recombining species microscopically. Excitonic recombination in a-Si:H has been discussed by many authors [see e.g. 17, 19-21]. And in fact, excitonic recombination could remove some of the difficulties with the radiative tunneling model. Measurements of optically detected magnetic resonance (ODMR) have shown that recombination in a-Si:H is strongly dependent on spin selection rules [21], but so far did not succeed in giving convincing proof of excitonic recombination.

4. Microscopic identification of the recombination channels

Recently new methods for studies of spin dependent recombination namely pulsed optically and electrically detected magnetic resonance (PEDMR and PODMR) have been introduced which may help to microscopically identify the character of the pairs [22]. For spin dependent recombination to occur the participating states have to be paramagnetic such that the spin selection rules determine the transition probabilities. Since the final state in the recombination transition is a singlet state, e-h pairs in singlet configuration will be able to rapidly recombine while recombination of triplet pairs will be prohibited by the spin selection rule. In a traditional measurement of optically detected magnetic resonance (ODMR) the photoluminescence intensity is recorded when the sample is brought into microwave resonance as in an ESR experiment. Recombination will be enhanced when triplet pairs are transformed into singlet pairs by microwave resonance which, in the simplest situation, results in either an enhancing resonance line when the radiative rate is enhanced or a quenching line when the non-radiative rate is enhanced. Such experiments give insight into the recombination dynamics and allow, in principle, to identify the participating centers by the g-values of the observed resonances. Various ODMR studies have led to the suggestion of excitonic recombination in a-Si:H [see e.g. 21]. However, the interpretation of the ODMR spectra turns out to be rather complicated. Often enhancing and quenching signals overlap and the influence of the experimental parameters (probing frequency, light intensity, microwave power, temperature) often led to conflicting observations.

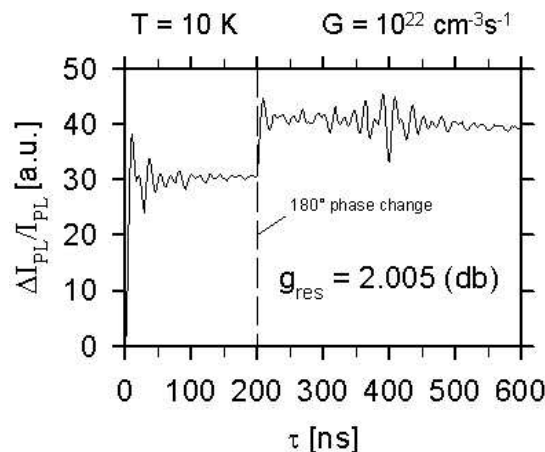


Fig. 8. Experimental PODMR transient of a-Si:H [23]. The magnetic field was chosen such that spins with a g-value of about 2.005 were at resonance. At $\tau = 200$ ns a phase change of 180° was introduced which creates a PL-echo at 400 ns.

The main difference of PODMR and the traditional ODMR is that in PODMR all spins are excited coherently by a high-power microwave pulse and can perform Rabi oscillations. The theory of such experiments has been treated by Böhme and Lips [22] using basic theory derived for the time-domain of spin-dependent recombination. The following hand-waving argument may be used to explain the principle considering the example of a weakly coupled e-h pair in triplet configuration. When a strong microwave burst is applied which is in resonance with the band tail electrons their spin will perform Rabi oscillations which means that the spin orientation will oscillate. The hole being only weakly coupled will not experience the microwave field such that the result is that the spin state of the pair will oscillate between singlet and triplet configuration. Therefore, the recombination rate performs oscillations which can be detected as an oscillating photoluminescence intensity. When the microwave stops after a time τ the actual spin state is frozen in and relaxation occurs by spin relaxation or recombination. The Rabi frequency f_{rabi} contains the information on the specific coupling of the recombining entities. It is proportional to the magnetic field of the pulse and the total spin. Therefore f_{rabi} it is twice as large for species with $S = 1$ than for $S = \frac{1}{2}$.

Fig. 8 displays an experimental PODMR measurement from the work of Lips, Böhme, and Ehara [23]. When a microwave pulse of length τ is applied there is an initial increase of the PL intensity followed by Rabi oscillations which clearly have various frequency components. The relevant information is the spectrum of Rabi frequencies [22, 23]. The amplitude of the Rabi oscillations decreases due to dephasing of the spins. In this experiment a 180° phase change of the microwave was introduced at $\tau = 200$ ns which makes the spins rotate in opposite direction such that after $\tau = 400$ ns the spins are in phase again. The result is an echo which exactly reproduces the original signal. This clearly shows that the observed behavior is due to Rabi oscillations and dephasing. Such transients were recorded varying the external magnetic field thus bringing the whole set of g-values between 1.97 and 2.05 into resonance. For each of the echo transients a fast Fourier transformation was performed to determine the Rabi frequencies and the involved g-values. The results of this procedure are summarized in Fig. 9. Clearly three different recombination channels are identified: (1) Non-radiative tunneling from band tail electrons into weakly coupled dangling bond states. (2) A single line at $g = 2.008$ involving a $S = 1$ triplet state due to excitons. (3) Recombination of strongly dipolar coupled electron hole pairs. It is estimated that the minimum inter-pair separation of these pairs is about 9 \AA while the average amounts to about 16 \AA .

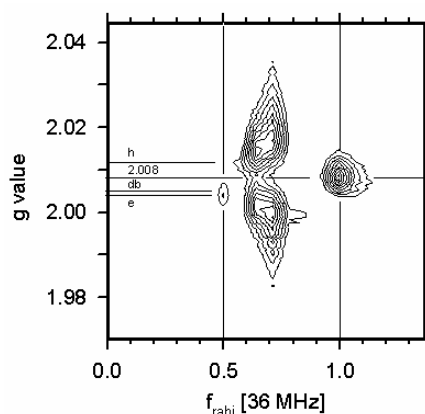


Fig. 9. Contour plot of the Rabi frequency f_{rabi} determined by fast Fourier transform (FFT) of a large set of echo transients which had been measured at various values of the magnetic field B_0 . B_0 is expressed in units of the g-value and f_{rabi} in units of the frequency of a $S = 1$ spin pair. The lines mark the g-values of the known ESR resonances.

Lips, Böhme and Ehara argue that both the exciton recombination and the recombination of strongly coupled e-h pairs are radiative processes. In view of the high generation rates of $G = 10^{22} \text{ cm}^{-3} \text{ s}^{-1}$ these experiments are clearly performed in the non-geminate recombination regime where

distant pair recombination is considered to prevail. The results from PODMR measurements unambiguously identify the recombination of excitons as an important radiative recombination channel and thus support to the revival of old suggestions [17, 19-21].

5. Conclusions

The kinetics of low-temperature recombination in a-Si:H are dominated by geminate recombination at low and moderate generation rates and by non-geminate recombination at high generation rates. The geminate process can be assigned to excitonic recombination with a lifetime distribution consisting of the components τ_1 and τ_2 . It is tempting to associate these components with the recombination of singlet (τ_2) and triplet (τ_1) excitons. Even at the lowest generation rates radiative recombination by distant pairs competes and finally becomes dominant for $G > 5 \times 10^{19} \text{ cm}^{-3} \text{ s}^{-1}$. In addition, at very high generation rates and very low temperatures ($T < 10 \text{ K}$) a non-radiative channel becomes competitive which has been assigned due to Auger recombination, the origin of which, however, still has not been fully clarified.

Acknowledgement

The author gratefully acknowledges valuable discussions with R. Stachowitz, C. Böhme and K. Lips.

References

- [1] R. C. Chittik, J. H. Alexander, H. F. Sterling, *J. Electrochem. Soc.* **116**, 77 – 81 (1969).
- [2] R. J. Loveland, W. E. Spear, A. Al-Shabaty, *J. of Non-Cryst. Solids* **13**, 55 – 68 (1973).
- [3] A. J. Lewis, G. A. N. Connell, W. Paul, J. Pawlik, R. Temkin, *AIP Conf. Proceed.* **20**, 27 – 33 (1974).
- [4] P. G. LeComber, W. E. Spear, *Solid State Commun.* **17**, 1193 (1975).
- [5] D. Carlson, C. R. Wronski, *Appl. Phys. Lett.* **28**, 671 – 673 (1976).
- [6] P. G. LeComber, W. E. Spear, A. Gaith, *Electronics Letters* **15**, 179 – 181 (1979).
- [7] R. A. Street, *Hydrogenated Amorphous Silicon*, Cambridge University Press, Cambridge, 1991.
- [8] R. A. Street (Ed), *Technology and Applications of Amorphous Silicon*, Springer Heidelberg (2000).
- [9] M. Hoheisel, R. Carius, W. Fuhs, *J. of Non-Cryst. Solids* **59/60**, 457 - 460 (1983).
- [10] S. D. Baranovskii, P. Thomas, G. J. Adriaenssens, *J. of Non-Cryst. Solids* **190**, 283 – 287 (1995).
- [11] R. A. Street, *Adv. in Physics* **30**, 593 – 676 (1981).
- [12] M. Bort, W. Fuhs, S. Liedke, R. Stachowitz, R. Carius, *Phil. Mag. Lett.* **64**, 227-233 (1991).
- [13] S. Ambros, R. Carius, H. Wagner, *J. of Non-Cryst. Solids* **137/138**, 555 (1991).
- [14] T. Aoki, T. Shimizu, S. Komodoori, S. Kobayashi, K. Shimakawa, *J. of Non-Cryst. Solids* **338 – 340**, 456 – 459 (2004).
- [15] B. I. Shklovskii, H. Fritzsche, S. D. Baranovskii, *Phys. Rev. Lett.* **62**, 2989 (1989).
- [16] E. J. Levin, S. Marianer, B. I. Shklovskii, *Phys. Rev. B*, 5906 (1992).
- [17] R. Stachowitz, M. Schubert, W. Fuhs, *J. of Non-Cryst. Solids* **227-230**, 190 (1998).
- [18] D. J. Dunstan, *Phil. Mag. B* **46**, 579 (1982).
- [19] D. Engemann, R. Fischer, in: *Amorphous and Liquid Semiconductors*, eds. J. Stuke and W. Brenig (Taylor & Francis, London 1974) 947.
- [20] B. A. Wilson, P. Hu, J. P. Harbison, T. M. Jedju, *Phys. Rev. Lett.* **50**, 1490 (1983).
- [21] K. Morigaki, *J. Non-Cryst. Solids* **77/78**, 583 (1985).
- [22] C. Böhme, K. Lips, *Phys. Rev. B* **68**, 245105 (2003).
- [23] K. Lips, C. Böhme, T. Ehara, *J. Optoelectron. Adv. Mater.* (in print 2005).